J Mater Sci (2011) 46:813–823
DOI 10.1007/s10853-010-4821-9

Photophysical and photocatalytic properties of novel Y_2GaSbO_7 and Y_2YbSbO_7 photocatalysts under visible light irradiation

Jingfei Luan · Kun Ma · Yongmei Li · Zhigang Zou

Received: 2 June 2010 / Accepted: 10 August 2010 / Published online: 24 August 2010

Abstract Y_2GaSbO_7 and Y_2YbSbO_7 were synthesized by solid state reaction method for the first time. The crystallinity, composition, bandgap, morphology, and grain size of Y_2GaSbO_7 and Y_2YbSbO_7 were characterized by a series of analytical techniques. The lattice parameter a for Y_2GaSbO_7 was found to be 10.17981(1) Å, and the lattice parameters for Y_2YbSbO_7 were found to be $a = 10.49741(9)$ Å, $b = 7.45088(3)$ Å, $c = 7.47148(7)$ Å, respectively. The values of band gap for Y_2GaSbO_7 and Y_2YbSbO_7 were calculated to be 2.245 and 2.521 eV, respectively. The photocatalytic degradation of rhodamine B (RhB) with Y_2GaSbO_7 or Y_2YbSbO_7 as photocatalyst was investigated under visible light irradiation. The results showed that Y_2GaSbO_7 and Y_2YbSbO_7 owned higher photocatalytic activity compared with Bi_2InTaO_7. Moreover, Y_2GaSbO_7 showed higher photocatalytic activity compared with Y_2YbSbO_7 for the photocatalytic degradation of RhB. The photocatalytic degradation of RhB followed the first-order reaction kinetics. The first-order rate constant, k, was 0.01817, 0.01341, and 0.00329 min^{-1} for Y_2GaSbO_7, Y_2YbSbO_7, and Bi_2InTaO_7, respectively. Complete removal of RhB was realized after visible light irradiation for 220 or 240 min with Y_2GaSbO_7 or Y_2YbSbO_7 as photocatalyst. The reduction of the total organic carbon and the evolution of CO_2 were also realized and these results indicated the continuous mineralization of RhB during the photocatalytic process with Y_2GaSbO_7 or Y_2YbSbO_7 as photocatalyst. The possible photocatalytic degradation pathway of RhB was revealed under visible light irradiation. Methylene blue and neutral red could be degraded efficiently with Y_2GaSbO_7 or Y_2YbSbO_7 as photocatalyst under visible light irradiation.

Introduction

N-containing dyes are extensively used in textile dying, paper printing, and other industrial processes. However, the effluent of N-containing dyes is extremely difficult to be removed owing to their resistance to conventional wastewater treatment processes such as biodegradation technology. Furthermore, N-containing dyes underwent natural reductive anaerobic degradation and potentially carcinogenic aromatic amines [1, 2] which caused a threat to human health were yielded. Photocatalysis is an environmental friendly technique compared with the traditional methods and dyes can be decomposed into water and carbon dioxide effectively by photocatalysis technique. In recent years, photocatalytic degradation of organic compounds was widely investigated in the field of environmental pollution control. As a result, related researches and developments were tremendous [3–22]. For photocatalytic process, photocatalysts are of great importance. Currently, most studies from researchers focused on novel photocatalysts and visible light response photocatalysts.

Among all kinds of N-containing dyes, rhodamine B (RhB) is an important representative dye. RhB was widely

J. Luan (✉) · K. Ma
State Key Laboratory of Pollution Control and Resource Reuse, School of the Environment, Nanjing University, Nanjing 210093, People's Republic of China
e-mail: jfluan@nju.edu.cn

Y. Li
State Key Laboratory of Pollution Control and Resource Reuse, School of the Environment, Tongji University, Shanghai 200092, People's Republic of China

Z. Zou
Eco-Materials and Renewable Energy Research Center, Nanjing University, Nanjing 210093, People's Republic of China

used as a colorant, a photosensitizer, and an active medium in dye lasers [23, 24]. Many researchers utilized RhB as a probe contaminant to evaluate the activity of a photocatalyst both under ultraviolet light irradiation [25–29] and under visible light irradiation [30–33].

In our published paper [34], Bi_2InTaO_7 which crystallized with the pyrochlore-type structure were found to have photocatalytic activity under visible light irradiation and it seemed to have potential for activity improvement upon modification of the structure of Bi_2InTaO_7. Along this line, it can be postulated that the substitution of Ta^{5+} by Sb^{5+}, the substitution of In^{3+} by Yb^{3+} or Ga^{3+}, and the substitution of Bi^{3+} by Y^{3+} may lead to an increase in carrier concentration and may result in the improvement of the photocatalytic properties. According to our work [35] and other researchers' work [36–38], the photocatalysts which contained the element of Y, Yb, Ga, or Sb showed high photocatalytic activity. Thus, we synthesized Y_2GaSbO_7 and Y_2YbSbO_7 for the first time and their structural, photophysical, and photocatalytic properties were investigated in detail. Moreover, a comparison of the photocatalytic properties among Y_2GaSbO_7, Y_2YbSbO_7, and Bi_2InTaO_7 was carried out to elucidate the structure–photocatalytic activity relationship in these newly synthesized compounds.

Experimental

Two novel photocatalysts, Y_2GaSbO_7 and Y_2YbSbO_7, were synthesized by solid state reaction method. Y_2O_3, Sb_2O_5, Ga_2O_3, Yb_2O_3, Bi_2O_3, In_2O_3, and Ta_2O_5 with purity of 99.99% (Sinopharm Group Chemical Reagent Co., Ltd, Shanghai, China) were used as raw materials. All powders were dried at 200 °C for 4 h before synthesis. In order to synthesize Y_2GaSbO_7, the precursors were stoichiometrically mixed, subsequently pressed into small columns, and put into an alumina crucible (Shenyang Crucible Co., LTD, China). Finally, the sample was calcined at 1320 °C for 65 h in an electric furnace (KSL 1700X, Hefei Kejing Materials Technology CO., LTD, China). Similarly, Y_2YbSbO_7 was prepared by calcination at 1320 °C for 65 h, and Bi_2InTaO_7 was prepared by calcination at 1050 °C for 46 h.

The crystal structures of the samples were analyzed by X-ray powder diffractometer (D/MAX-RB, Rigaku Co., Japan) with CuKα radiation ($\lambda = 1.54056$). The particle sizes of the photocatalysts were measured by Malvern's mastersize-2000 particle size analyzer (Malvern Instruments Ltd, UK). The particle morphology of the photocatalysts was measured by transmission electron microscope (TEM, Tecnal F20 S-Twin, FEI Corporation, USA). The chemical composition of the photocatalysts was determined by scanning electron microscope-X-ray energy dispersion spectrum (SEM–EDS, LEO 1530VP, LEO Corporation, Germany). The O^{2-}, Y^{3+}, Ga^{3+}, Yb^{3+}, and Sb^{5+} contents of Y_2GaSbO_7 and Y_2YbSbO_7 were determined by X-ray photoelectron spectroscopy (XPS, ESCALABMK-2, VG Scientific Ltd, UK). The optical absorption was examined by UV–vis spectrophotometer (Lambda 40, Perkin-Elmer Co., USA). The surface areas were measured by the Brunauer–Emmett–Teller (BET) method (MS-21, Quantachrome Instruments Co., USA) with N_2 adsorption at liquid nitrogen temperature.

The photocatalytic degradation of RhB (Tianjin Kermel Chemical Reagent Co., Ltd) was carried out by suspending 0.8 g Y_2GaSbO_7, Y_2YbSbO_7, or Bi_2InTaO_7 powder within 300 mL RhB, methylene blue (MB), or neutral red (NR) solution of 0.0293 mM with a pyrex glass cell. Before visible light irradiation, the suspensions were magnetically stirred in the dark for 45 min to get the equilibrium of adsorption and desorption. The reactor was composed of a 300 W Xe arc lamp with the main emission wavelength at 436 nm (Nanjing JYZCPST Co., LTD), a magnetic stirrer and a cut-off filter ($\lambda > 400$ nm). The Xe arc lamp which was surrounded by a quartz jacket was placed within the inner part of a reactor quartz vessel (5.8 cm in diameter and 68 cm in length), through which a suspension of RhB and the photocatalyst was circulated. An outer recycling water glass jacket maintained a constant reaction temperature (22 °C). Throughout the experiment, the solution was continuously stirred and aerated. pH adjustment was not made and the initial pH value was 7.0. 2 mL aliquots were sampled at various time intervals. The incident photon flux I_o which was measured by a radiometer (Model FZ-A, Photoelectric Instrument Factory Beijing Normal University, China) was determined to be 4.76×10^{-6} Einstein L^{-1} s^{-1} under visible light irradiation (wavelength range of 400–700 nm). The incident photon flux on the reactor was varied by adjusting the distance between the reactor and the Xe arc lamp. The concentration of RhB was determined according to the absorption at 553.5 nm which was measured by an UV–vis spectrophotometer (Lambda 40, Perkin-Elmer Corporation, USA). The concentration of MB was determined according to the absorption at 664 nm and the concentration of NR was determined according to the absorption at 526 nm. The inorganic products which were obtained from RhB degradation were analyzed by ion chromatograph (DX-300, Dionex Corporation, USA). The identification and the degradation intermediate products of RhB were measured by liquid chromatograph–mass spectrometer (LC–MS, Thermo Quest LCQ Duo, USA, Beta Basic-C_{18} HPLC column: 150 × 2.1 mm, ID of 5 μm, Finnigan, Thermo, USA). Here, 20 μL of post-photocatalysis solution was injected automatically into the LC–MS system. The eluent contained 60% methanol and 40% water, and the flow rate was 0.2 mL min^{-1}. MS conditions

contained an electrospray ionization interface, a constant sheath gas flow rate, a capillary temperature of 27 °C with a voltage of 19.00 V and a spray voltage of 5000 V. The spectrum was acquired in the negative ion scan mode and the $m\ z^{-1}$ range was swept from 50 to 600. Evolution of CO_2 was analyzed with an intersmat™ IGC120-MB gas chromatograph which was equipped with a porapack Q column (3 m in length and an inner diameter of 0.25 in.) which was connected to a catharometer detector.

The total organic carbon (TOC) concentration was determined by a TOC analyzer (TOC-5000, Shimadzu Corporation, Japan). The photonic efficiency was calculated according to the following equation [39, 40]:

$$\varphi = R/I_o$$

where φ is the photonic efficiency (%), and R is the degradation rate of RhB (mol L^{-1} s^{-1}), and I_o is the incident photon flux (Einstein L^{-1} s^{-1}).

Results and discussion

Characterization

TEM images (Fig. 1) show the typical texture and morphology of Y_2GaSbO_7 and Y_2YbSbO_7. The mean particle size was 276 nm for Y_2GaSbO_7 and 312 nm for Y_2YbSbO_7. The X-ray diffraction patterns of Y_2GaSbO_7 and Y_2YbSbO_7 are shown in Figs. 2 and 3, respectively. It could be seen from Figs. 2 and 3 that the full-profile structure refinements of the collected data were also obtained by the RIETAN™ [41] program which was based on Rietveld analysis. The X-ray diffraction patterns indicated that Y_2GaSbO_7 and Y_2YbSbO_7 were both single phases. As to Y_2GaSbO_7, the refinement results indicated a good agreement between the observed and calculated intensities for the pyrochlore-type structure and a cubic crystal system with a space group *Fd3m* (O atoms were included in the model). At the same time, the crystal structure of the orthorhombic fluorite-related compound Y_2YbSbO_7 with a space group $C222_1$ (O atoms were included in the model) had been determined according to the refinement results. Sm_3SbO_7 [42] was also found to be orthorhombic fluorite-related compound with a space group $C222_1$. The lattice parameter a for Y_2GaSbO_7 was found to be 10.17981(1) Å, and the lattice parameters for Y_2YbSbO_7 were found to be $a = 10.49741(9)$ Å, $b = 7.45088(3)$ Å, $c = 7.47148(7)$ Å, respectively. All the diffraction peaks for Y_2GaSbO_7 and Y_2YbSbO_7 could be successfully indexed according to the lattice constant and above refinement results. The atomic coordinates and structural parameters of Y_2GaSbO_7 and Y_2YbSbO_7 are listed in Tables 1 and 2, respectively. It could be seen from the XRD results that 2 theta angles of each reflection of Y_2GaSbO_7 changed with Ga^{3+} being substituted by Yb^{3+}. The lattice parameter increased from $a = 10.17981(1)$ Å

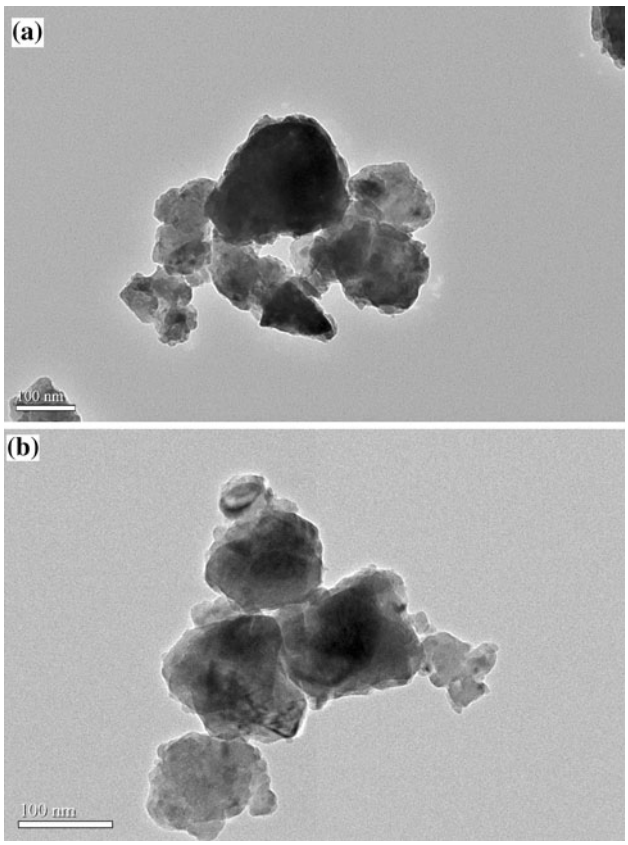

Fig. 1 TEM images of **a** Y_2GaSbO_7 and **b** Y_2YbSbO_7

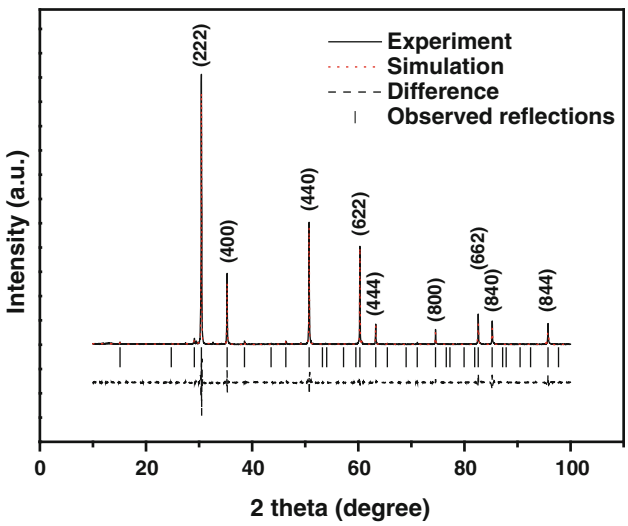

Fig. 2 X-ray powder diffraction patterns and Rietveld refinements of Y_2GaSbO_7. A difference (observed-calculated) profile is shown beneath. The *tick marks* represent reflection positions

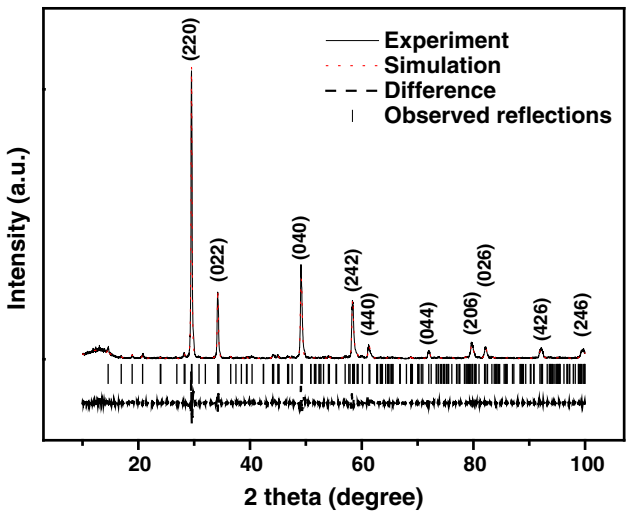

Fig. 3 X-ray powder diffraction patterns and Rietveld refinements of Y_2YbSbO_7. A difference (observed-calculated) profile is shown beneath. The *tick marks* represent reflection positions

Table 1 Structural parameters of Y_2GaSbO_7

Atom	*x*	*y*	*z*	Occupancy
Y	0.0000000	0.0000000	0.0000000	1.0
Ga	0.5000000	0.5000000	0.5000000	0.5
Sb	0.5000000	0.5000000	0.5000000	0.5
O(1)	−0.1867380	0.1250000	0.1250000	1.0
O(2)	0.1250000	0.1250000	0.1250000	1.0

Table 2 Structural parameters of Y_2YbSbO_7

Atom	*x*	*y*	*z*	Occupancy
Y	0.2397110	0.2518870	0.0080500	1.0
Yb	0.0000000	0.5327660	0.2500000	1.0
Sb	0.0000000	0.0012715	0.2500000	1.0
O(1)	0.1729340	0.2109000	0.2311260	1.0
O(2)	0.1744140	0.7481370	0.2835330	1.0
O(3)	0.0358980	0.5000000	0.0000000	1.0
O(4)	0.0829680	0.5000000	0.5000000	1.0
O(5)	0.0919565	0.0000000	0.0000000	1.0

for Y_2GaSbO_7 to $a = 10.49741(9)$ Å for Y_2YbSbO_7, which indicated a decrease for lattice parameter *a* of the photocatalyst with decrease of the ionic radii, Ga^{3+} (0.62 Å) < Yb^{3+} (0.985 Å).

The XRD patterns showed that the pyrochlore-type structure of Y_2GaSbO_7 was the same with the structure of Bi_2InTaO_7. The cubic system structure with space group *Fd3m* for Bi_2InTaO_7 kept unchanged with Ta^{5+} being substituted by Sb^{5+}, In^{3+} being substituted by Ga^{3+} and Bi^{3+} being substituted by Y^{3+}. However, the cubic system structure with space group *Fd3m* for Bi_2InTaO_7 was turned to the orthorhombic fluorite-related compound Y_2YbSbO_7 which owned a space group $C222_1$ with Ta^{5+} being substituted by Sb^{5+}, In^{3+} being substituted by Yb^{3+} and Bi^{3+} being substituted by Y^{3+}. The refinement outcome for Y_2GaSbO_7 generated the unweighted *R* factors and R_P was equal to 12.36%. Similarly, the unweighted R_P factor for Y_2YbSbO_7 was equal to 8.22%. Zou et al. [43] refined the crystal structure of Bi_2InNbO_7 and obtained a large *R* factor for Bi_2InNbO_7, which was due to a slightly modified structure model for Bi_2InNbO_7. According to the high purity of the precursors that we used, it was unlikely that the observed space groups originated from the presence of impurities. Therefore, it could be concluded that the slightly high *R* factors for Y_2GaSbO_7 or Y_2YbSbO_7 were owing to a slightly modified structure model of Y_2GaSbO_7 or Y_2YbSbO_7. It should be emphasized that the defects or the disorder/order of a fraction of the atoms could result in the change of the structures such as different bond-distance distributions, thermal displacement parameters, and/or occupancy for some of the atoms.

The XPS spectra of Y_2GaSbO_7 and Y_2YbSbO_7 were measured. Various elemental peaks which are corresponding to specific binding energies are provided in Table 3. The results further suggested that the oxidation states of Y, Ga, Yb, Sb, and O ions from Y_2GaSbO_7 or Y_2YbSbO_7 were +3, +3, +3, +5, and −2, respectively. According to our XPS and SEM–EDS results, the average atomic ratios of Y:Ga:Sb:O were 2.00:0.96:1.03:6.97 for Y_2GaSbO_7 and the average atomic ratios of Y:Yb:Sb:O were 2.00:1.02:0.96:6.98 for Y_2YbSbO_7. Thus, it could be deduced that Y_2GaSbO_7 and Y_2YbSbO_7 were of high purity under our preparation conditions. It was noteworthy that neither shoulders nor widening of any XPS peaks of Y_2GaSbO_7 or Y_2YbSbO_7 were observed, suggesting (albeit not proving) the absence of any other phases.

The absorption spectra of Y_2GaSbO_7 and Y_2YbSbO_7 are shown in Fig. 4. The results suggested that the absorption edges of Y_2GaSbO_7 and Y_2YbSbO_7 were at 576 and 442 nm, respectively. It was noteworthy that the apparent absorption (defined hereby as 1-transmission) could not take into consideration about reflection and scattering. As a consequence, the apparent absorbance at sub-bandgap wavelengths (376–800 nm for Y_2GaSbO_7, and 428–800 nm for Y_2YbSbO_7) was higher than zero. For a crystalline semiconductor, the optical absorption near the band edge follows the equation: [44, 45]

$$\alpha h\nu = A(h\nu - E_g)^n$$

Here, *A*, α, E_g, and ν are proportional constant, absorption coefficient, band gap, and light frequency, respectively. Within this equation, *n* determines the character of the transition in a semiconductor. According to the equation,

Table 3 Binding energies (BE) for key elements

Compound	$Ga_{2p3/2}$ BE (eV)	$Sb_{3d5/2}$ BE (eV)	$Y_{3d5/2}$ BE (eV)	$Yb_{4p3/2}$ BE (eV)	O_{1s} BE (eV)
Y_2YbSbO_7		530.92	156.88	346.52	529.95
Y_2GaSbO_7	1117.52	530.86	156.75		530.22

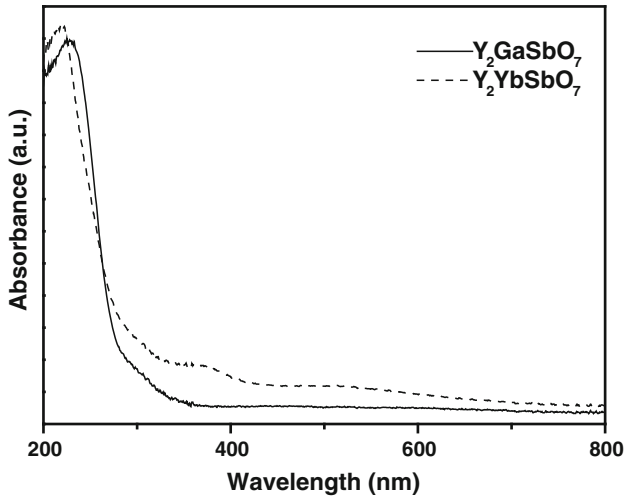

Fig. 4 UV–vis absorption spectra of Y_2GaSbO_7 and Y_2YbSbO_7

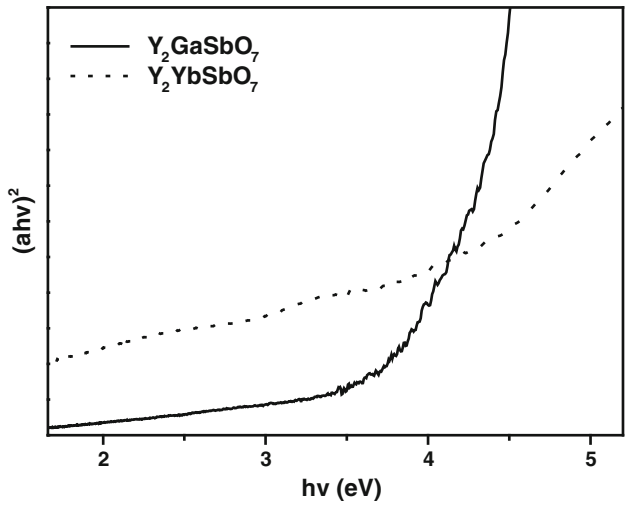

Fig. 5 Plot of $(\alpha hv)^2$ versus hv for Y_2GaSbO_7 and Y_2YbSbO_7

the plot (Fig. 5) of $(\alpha hv)^{1/n}$ which is a function of hv for Y_2GaSbO_7 and Y_2YbSbO_7 is made. The n values of Y_2GaSbO_7 and Y_2YbSbO_7 were calculated to be 0.54 and 0.62, respectively. The values of E_g for Y_2GaSbO_7 and Y_2YbSbO_7 were calculated to be 2.245 and 2.521 eV, respectively, indicating that Y_2GaSbO_7 possessed narrower band gap than Y_2YbSbO_7 and the optical transition for Y_2YbSbO_7 or Y_2GaSbO_7 was directly allowed.

Photocatalytic activity

The temporal spectral changes of aqueous RhB solutions under visible light ($\lambda > 400$ nm) irradiation in the presence of Y_2GaSbO_7 or Y_2YbSbO_7 are presented in Fig. 6. The measurements were performed under oxygen-saturation conditions ($[O_2]_{sat} = 1.02 \times 10^{-3}$ M). Under the condition of darkness, the degradation of RhB did not occur with the photocatalysts or without the photocatalysts. As presented in Fig. 6, the reduction of typical RhB showed a maximum adsorption peak at 553.5 nm. The absorption peaks decreased to a low value with Y_2GaSbO_7 or Y_2YbSbO_7 as photocatalyst after 200 min, indicating the voluminous degradation of RhB.

The changes of RhB concentration which are deduced from the UV–vis spectra are presented in Fig. 7. After visible light irradiation for 200 min, 97.3%, 90.2%, or 45.1% of RhB was removed with Y_2GaSbO_7, Y_2YbSbO_7, or Bi_2InTaO_7 as photocatalyst, respectively. The degradation rate of RhB was about 2.376×10^{-9} mol L^{-1} s^{-1} and

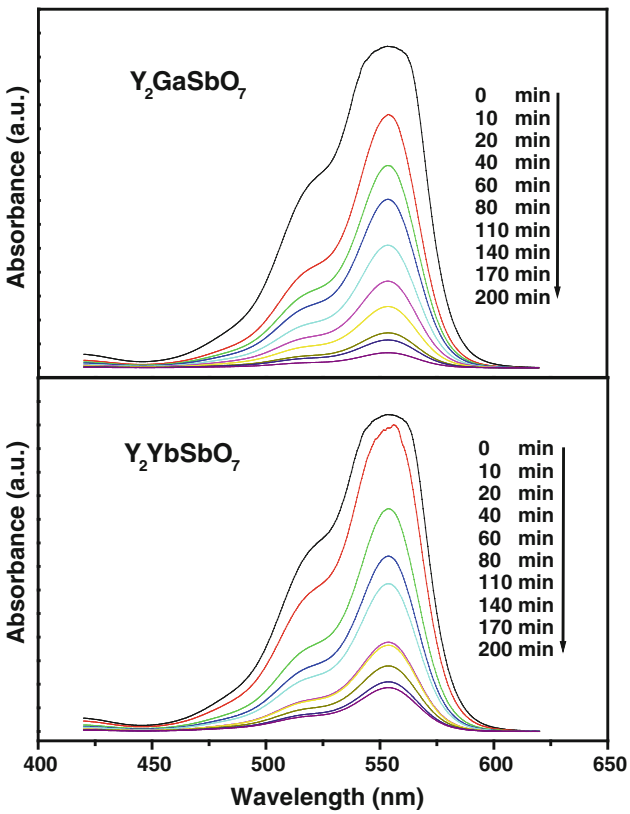

Fig. 6 Temporal spectral changes of aqueous solutions of RhB due to visible light irradiation in the presence of Y_2GaSbO_7 or Y_2YbSbO_7

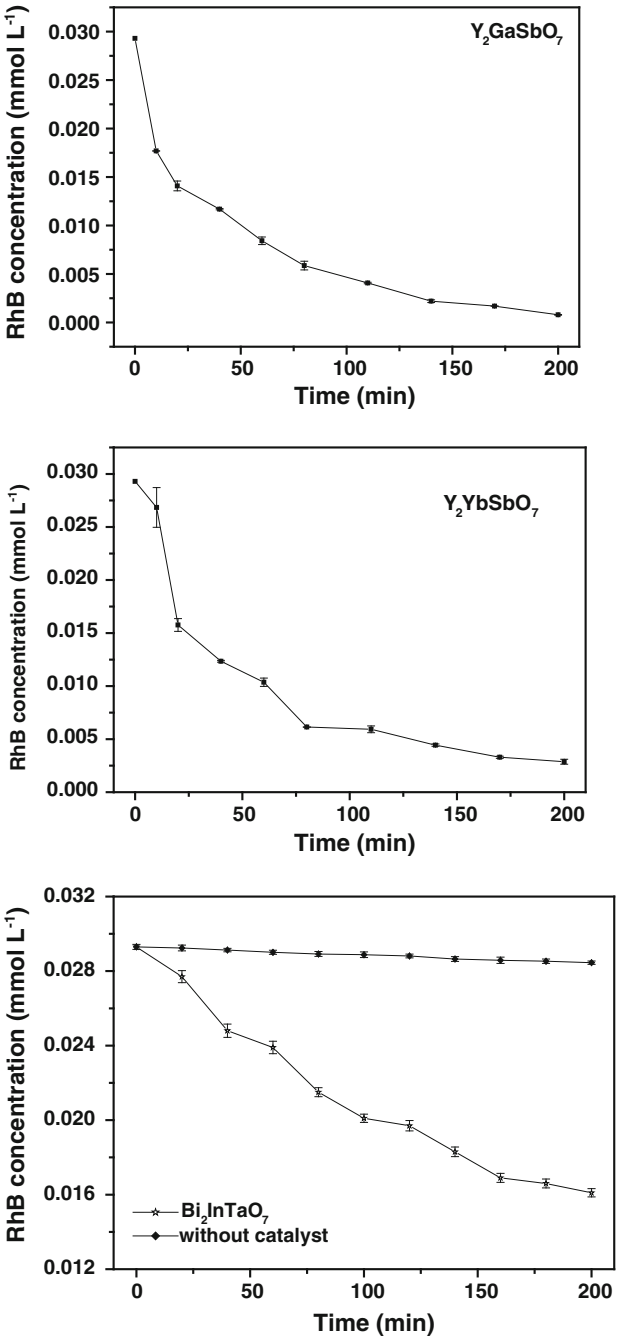

Fig. 7 Photocatalytic degradation of RhB under visible light irradiation in the presence of Y_2GaSbO_7, Y_2YbSbO_7, Bi_2InTaO_7 as well as in the absence of photocatalysts

the initial photonic efficiency was estimated to be 0.0499% ($\lambda = 420$ nm) with Y_2GaSbO_7 as photocatalyst. Similarly, the degradation rate of RhB was about 2.202×10^{-9} mol L^{-1} s^{-1} and the initial photonic efficiency was estimated to be 0.0463% ($\lambda = 420$ nm) with Y_2YbSbO_7 as photocatalyst. In contrast, the photocatalytic efficiency with Bi_2InTaO_7 as photocatalyst was inferior to the photocatalytic efficiency with Y_2GaSbO_7 or Y_2YbSbO_7 as

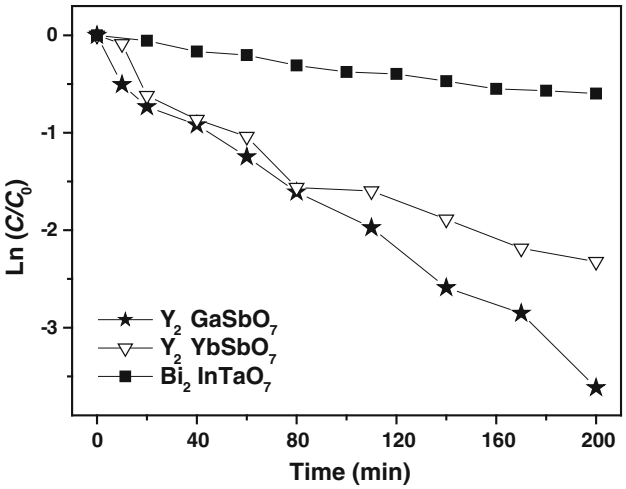

Fig. 8 First-order kinetic plots for the photocatalytic degradation of RhB with Y_2GaSbO_7, Y_2YbSbO_7, and Bi_2InTaO_7 as photocatalysts

photocatalyst. For example, the RhB concentration decreased only from 0.0293 mM to 0.0161 mM with Bi_2InTaO_7 as photocatalyst within 200 min and the degradation rate of RhB was less than 1.1×10^{-9} mol L^{-1} s^{-1}. The initial photonic efficiency was estimated to be 0.0231% ($\lambda = 420$ nm) with Bi_2InTaO_7 as photocatalyst. Based on above results, fast degradation rate was observed with Y_2GaSbO_7 or Y_2YbSbO_7 as photocatalyst. Moreover, the photocatalytic degradation activity of Y_2GaSbO_7 or Y_2YbSbO_7 was higher than that of Bi_2InTaO_7. Furthermore, the photocatalytic degradation activity of Y_2GaSbO_7 was higher than that of Y_2YbSbO_7. As expected, the reduction of RhB concentration was pimping in the absence of the photocatalyst. The degradation rate of RhB was about 0.0708×10^{-9} mol L^{-1} s^{-1} and the photonic efficiency was 0.00149% ($\lambda = 420$ nm) after visible light irradiation of 200 min in the absence of the photocatalyst and it was suggested that the observed disappearance of RhB was owing to direct dye-sensitization and the results were similar to the observations from Zhao and co-workers [46] who studied alizarin red and X3B dyes.

The kinetic curves which represent the photocatalytic degradation results of RhB with Y_2GaSbO_7, Y_2YbSbO_7 and Bi_2InTaO_7 as photocatalysts are demonstrated in Fig. 8. A good linear correlation between ln (C/C_o) and the irradiation time could be seen from Fig. 8 and it suggested that the reaction kinetics followed a pseudo-first-order rate law. As to ln (C/C_o), C represents the RhB concentration at time t, and C_o represents the initial RhB concentration. According to the relationship between ln (C/C_o) and the irradiation time, the apparent first-order rate constant, k, was estimated to be 0.01817 min^{-1} with Y_2GaSbO_7 as photocatalyst, 0.01341 min^{-1} with Y_2YbSbO_7 as photocatalyst, and 0.00329 min^{-1} with Bi_2InTaO_7 as photocatalyst, indicating that Y_2GaSbO_7 or Y_2YbSbO_7 was more suitable than

Bi_2InTaO_7 for the photocatalytic degradation of RhB under visible light irradiation. At the same time, Y_2GaSbO_7 was more suitable than Y_2YbSbO_7 for the photocatalytic degradation of RhB under visible light irradiation.

The photodegradation intermediate products of RhB in our experiment were identified as 3-nitrobenzoic acid (*m*/*z*:167), phthalic anhydride (m/z:148), pentanedioic acid, phthalic acid (*m*/*z*:166), and 2-hydroxypentanedioic (*m*/*z*:132). A possible degradation pathway of RhB is proposed in Fig. 9 according to the detected intermediate products. This degradation pathway for RhB was similar but not the same with the degradation pathway which was proposed by Horikoshi et al. [47]. According to the research results from Zhang and co-workers [33], the photodegradation of RhB occurred via two competitive processes: the first process was N-demethylation, and the second process was the destruction of the conjugated structure. Thus, we considered that chromophore cleavage, opening-ring, and mineralization would be the main degradation pathway of RhB in our experiment. RhB was converted into smaller organic species and ultimately mineralized into inorganic products such as CO_2 and H_2O. The yield of CO_2 during the photocatalytic degradation process of RhB is shown in Fig. 10. The results showed that the yield of CO_2 increased with increasing irradiation time. In addition, the production rate of CO_2 with Y_2GaSbO_7 or Y_2YbSbO_7 as photocatalyst was higher than that with Bi_2InTaO_7 as photocatalyst and above results were in line with the absorption curves of Y_2GaSbO_7 or Y_2YbSbO_7 (Fig. 4). For example, the yield of CO_2 was 0.2334, 0.2099, or 0.1080 mmol with Y_2GaSbO_7, Y_2YbSbO_7, or Bi_2InTaO_7 as photocatalyst under visible light irradiation of 200 min.

The total organic carbon (TOC) changes of the RhB solution are shown in Fig. 11. The results showed that 94.87% or 85.32% of TOC decrease was obtained after visible light irradiation of 200 min with Y_2GaSbO_7 or Y_2YbSbO_7 as photocatalyst, indicating that abundant

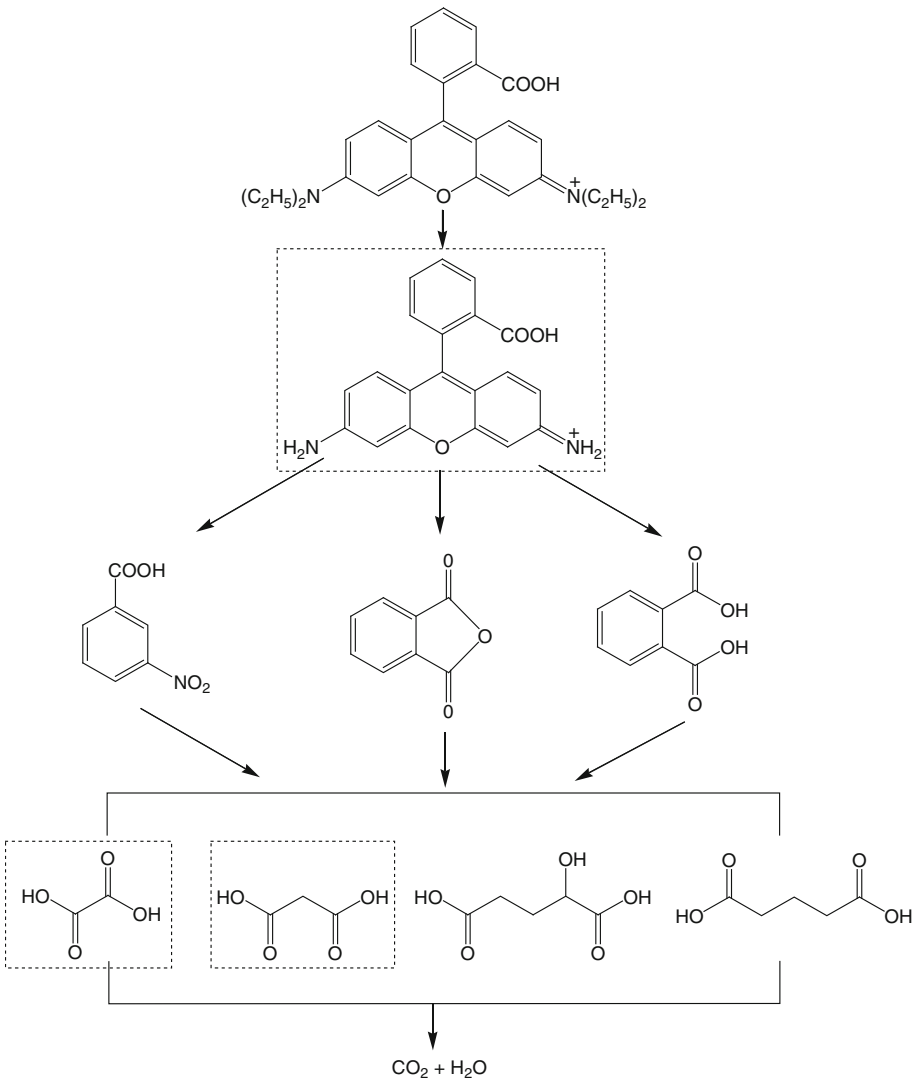

Fig. 9 Suggested photocatalytic degradation pathway scheme for RhB under visible light irradiation (*dotted line*: deduced intermediates)

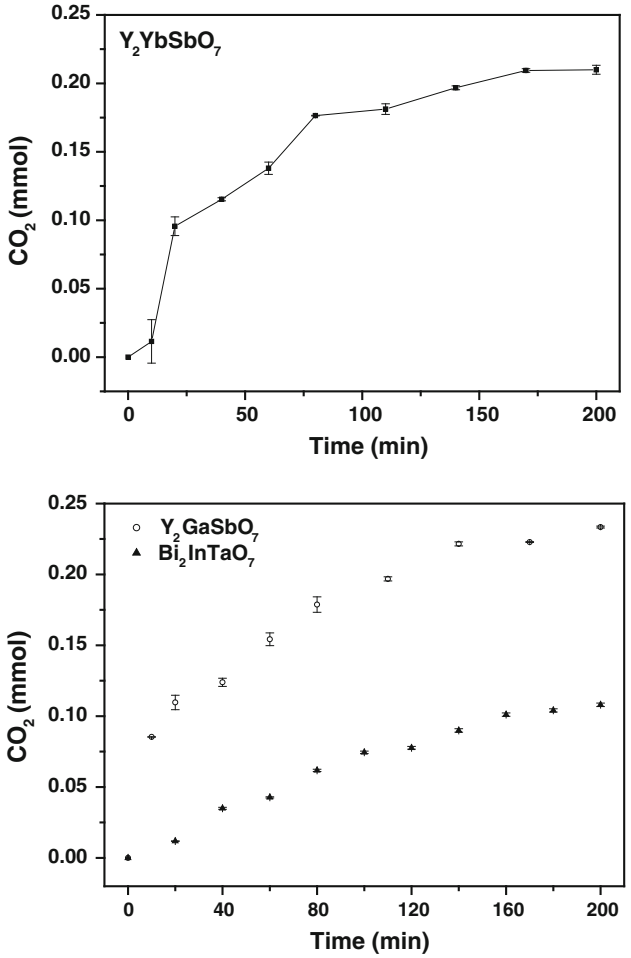

Fig. 10 The yield of CO_2 during the photocatalytic degradation of RhB under visible light irradiation with Y_2GaSbO_7, Y_2YbSbO_7, and Bi_2InTaO_7 as photocatalysts

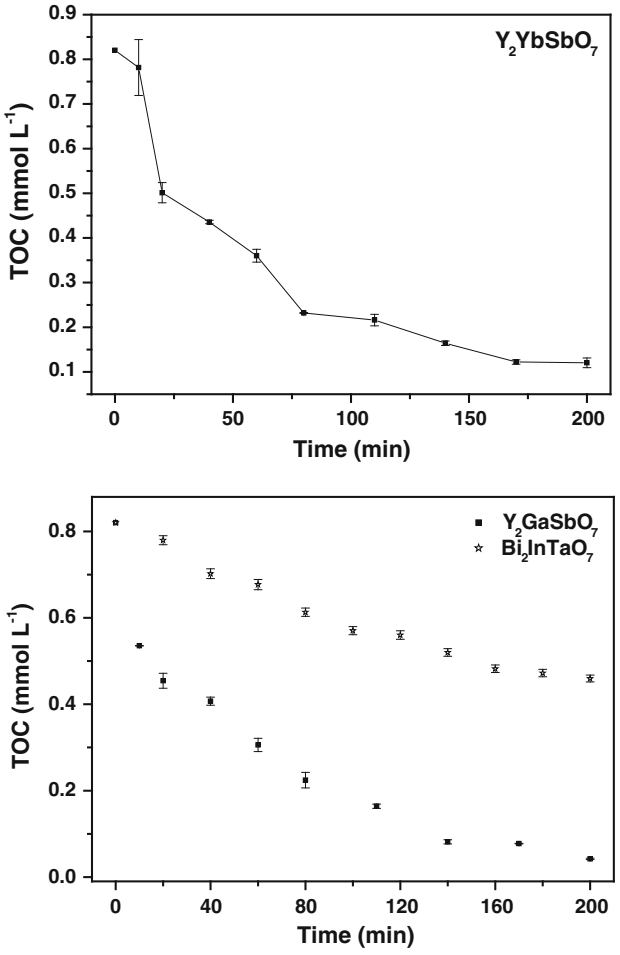

Fig. 11 Disappearance of the TOC during the photocatalytic degradation of RhB under visible light irradiation with Y_2GaSbO_7, Y_2YbSbO_7, and Bi_2InTaO_7 as photocatalysts

mineralization of RhB was achieved. Moreover, only 43.98% of TOC decrease was obtained with Bi_2InTaO_7 as photocatalyst after visible light irradiation of 200 min.

The photocatalytic activities of Y_2GaSbO_7 and Y_2YbSbO_7 were remarkable under visible light irradiation. This superior quality could be more significant if we considered the fact that the specific surface area of Y_2GaSbO_7 or Y_2YbSbO_7 was much smaller than that of degussa P25. In our experiment, the specific surface area which was detected by the BET isotherm measurements was 3.84, 3.52, or 1.26 $m^2\ g^{-1}$ for Y_2GaSbO_7, Y_2YbSbO_7, or Bi_2InTaO_7, respectively. It could be seen that the surface area of Y_2GaSbO_7 or Y_2YbSbO_7 was about 14 times smaller than that of P25 which was measured to be 50 $m^2\ g^{-1}$.

The first reason that Y_2GaSbO_7 and Y_2YbSbO_7 showed good photocatalytic activity under visible light irradiation could be attributed to the effect of photosensitization by RhB itself in the visible light region (Scheme I).

$$\text{Scheme I}: \mathrm{RhB_{(ads)}} \xrightarrow{\text{Visible light}} \mathrm{RhB^{*}_{(ads)}} \quad (1)$$

$$\mathrm{RhB^{*}_{(ads)}} + \mathrm{Y_2GaSbO_7/Y_2YbSbO_7} \rightarrow \mathrm{Y_2GaSbO_7/Y_2YbSbO_7(e)} + \mathrm{RhB^{+}_{(ads)}} \quad (2)$$

$$\mathrm{Y_2GaSbO_7/Y_2YbSbO_7(e)} + \mathrm{O_2} \rightarrow \mathrm{Y_2GaSbO_7/Y_2YbSbO_7} + \mathrm{\cdot O_2^{-}} \quad (3)$$

According to this mechanism, RhB which was adsorbed on Y_2GaSbO_7 or Y_2YbSbO_7 was excited by visible light irradiation. Subsequently, an electron was injected from the excited RhB to the conduction band of Y_2GaSbO_7 or Y_2YbSbO_7 where the electron was scavenged by molecular oxygen. Scheme I explained the results which were obtained with Y_2GaSbO_7 or Y_2YbSbO_7 as photocatalyst under visible light irradiation, where Y_2GaSbO_7 or Y_2YbSbO_7 might serve to reduce recombination via the scavenging of electrons [48]. The second reason that Y_2GaSbO_7 and Y_2YbSbO_7 showed good photocatalytic activity under visible light irradiation could be attributed to

the band gap excitation of Y_2GaSbO_7 or Y_2YbSbO_7 because the absorption edges of Y_2GaSbO_7 and Y_2YbSbO_7 were 576 and 442 nm (Scheme II). Within visible light region, the mechanism which was responsible for the photodegradation of RhB went through band gap excitation of Y_2GaSbO_7 or Y_2YbSbO_7. Although detailed experiments about the effect of oxygen and water on the degradation mechanism were not performed, it was sensible to assume that the mechanism in this step was similar to the mechanism which was observed for Y_2GaSbO_7 or Y_2YbSbO_7 under supra-bandgap irradiation, namely Scheme II:

$$\text{Scheme II}: Y_2GaSbO_7/Y_2YbSbO_7 \xrightarrow{\text{Visible light}} h^+ + e^- \quad (4)$$

$$e^- + O_2 \rightarrow {}^{\cdot}O_2^- \quad (5)$$

$$h^+ + OH^- \rightarrow {}^{\cdot}OH \quad (6)$$

Previous luminescent studies had shown that the closer the M–O–M bond angle was to 180°, the more easily the excited state could delocalize [49], the more easily the charge carriers could move in the matrix. The mobility of the photoinduced electrons and holes influenced the photocatalytic activity because high diffusivity indicated the improvement of the probability that the photogenerated electrons and holes would reach the reactive sites of the photocatalyst surface quickly. As to Y_2YbSbO_7, the Yb–O–Sb bond angle was 111.422°. Meanwhile, as to Y_2GaSbO_7, the Ga–O–Sb bond angle was 125.458°. Above results indicated that the Yb–O–Sb or Ga–O–Sb bond angle of Y_2YbSbO_7 or Y_2GaSbO_7 was close to 180°, thus the photocatalytic activity of Y_2GaSbO_7 or Y_2YbSbO_7 was consequently high. In addition, the Ga–O–Sb bond angle of Y_2GaSbO_7 was larger than the Yb–O–Sb bond angle of Y_2YbSbO_7, which resulted in an increase of the photocatalytic activity of Y_2GaSbO_7 compared with that of Y_2YbSbO_7. The crystal structure of Y_2GaSbO_7 was the same as Bi_2InTaO_7, but the crystal structure of Y_2YbSbO_7 was different from that of Bi_2InTaO_7. In addition, the electronic structures of Y_2GaSbO_7 and Y_2YbSbO_7 were different from that of Bi_2InTaO_7. As to Y_2GaSbO_7 and Y_2YbSbO_7, Y was 4*d*-block rare earth metal element, and Ga was 4*p*-block metal element, and Yb was 4*f*-block metal element, and Sb was 5*p*-block metal element. But as to Bi_2InTaO_7, Ta was 5*d*-block metal element, and In was 5*p*-block metal element, and Bi was 6*p*-block metal element, indicating that the photocatalytic activity of the photocatalyst might be affected by not only the crystal structure of the photocatalyst but also the electronic structure of the photocatalyst. According to above analysis, the difference of RhB photodegradation effect among Y_2GaSbO_7, Y_2YbSbO_7, and Bi_2InTaO_7 could be attributed mainly to the difference of their crystalline structure and electronic structure.

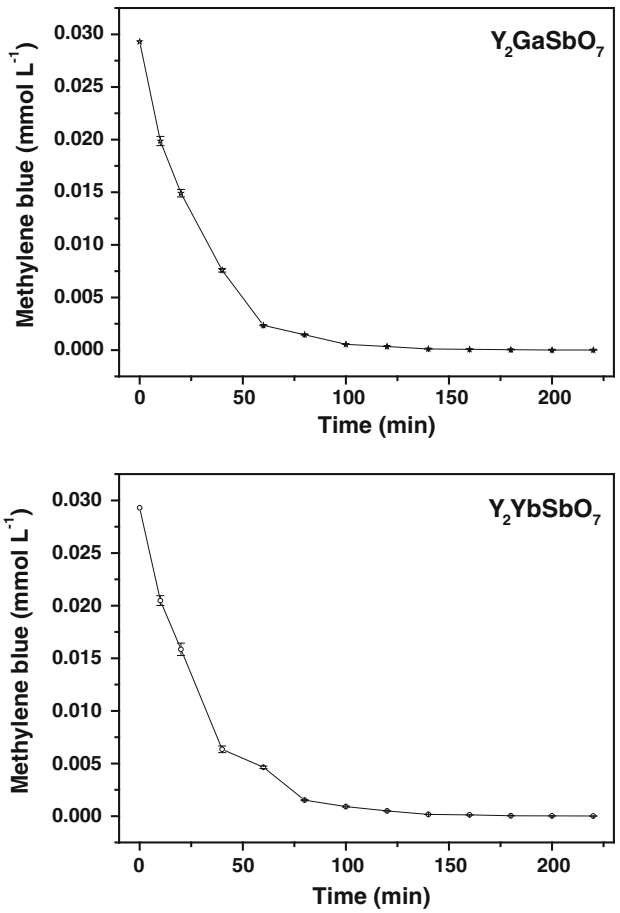

Fig. 12 Photocatalytic degradation of MB under visible light irradiation in the presence of Y_2GaSbO_7 and Y_2YbSbO_7

In order to show the photocatalytic degradation results of other dyes with Y_2GaSbO_7 or Y_2YbSbO as photocatalyst, MB and NR were degraded under visible light irradiation in the presence of Y_2GaSbO_7 or Y_2YbSbO_7. Figure 12 shows the photocatalytic degradation results of MB under visible light irradiation in the presence of Y_2GaSbO_7 and Y_2YbSbO_7. After visible light irradiation of 200 min, 99.97% or 99.91% of MB was removed with Y_2GaSbO_7 or Y_2YbSbO_7 as photocatalyst. The degradation rate of MB was about 2.441×10^{-9} mol L^{-1} s^{-1} and the initial photonic efficiency was estimated to be 0.0513% ($\lambda = 420$ nm) with Y_2GaSbO_7 as photocatalyst. Similarly, the degradation rate of MB was about 2.439×10^{-9} mol L^{-1} s^{-1} and the initial photonic efficiency was estimated to be 0.0512% ($\lambda = 420$ nm) with Y_2YbSbO_7 as photocatalyst. Figure 13 shows the photocatalytic degradation results of NR under visible light irradiation in the presence of Y_2GaSbO_7 and Y_2YbSbO_7. After visible light irradiation of 200 min, 99.83% or 99.64% of NR was removed with Y_2GaSbO_7 or Y_2YbSbO_7 as photocatalyst. The degradation rate of NR was about 2.437×10^{-9} mol L^{-1} s^{-1} and the initial photonic efficiency was

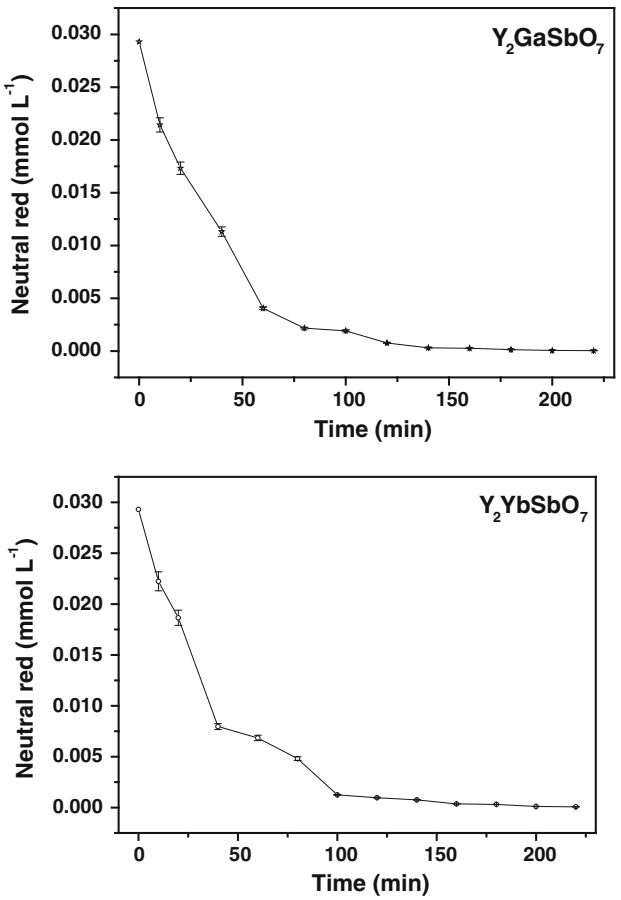

Fig. 13 Photocatalytic degradation of NR under visible light irradiation in the presence of Y_2GaSbO_7 and Y_2YbSbO_7

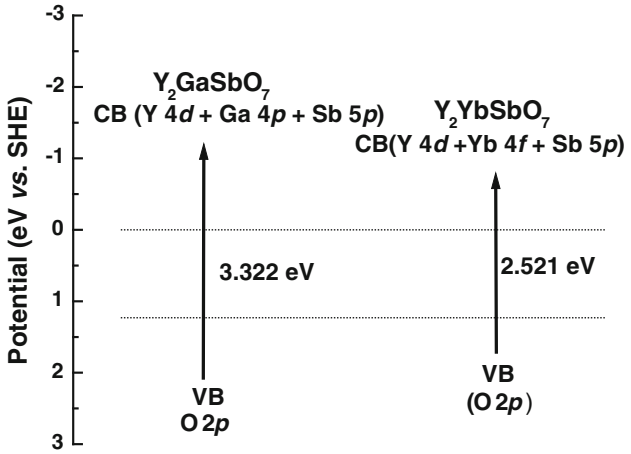

Fig. 14 Suggested band structures of Y_2GaSbO_7 and Y_2YbSbO_7

estimated to be 0.0512% ($\lambda = 420$ nm) with Y_2GaSbO_7 as photocatalyst. Similarly, the degradation rate of NR was about 2.433×10^{-9} mol L^{-1} s^{-1} and the initial photonic efficiency was estimated to be 0.0511% ($\lambda = 420$ nm) with Y_2YbSbO_7 as photocatalyst.

The suggested band structures of Y_2GaSbO_7 and Y_2YbSbO_7 are shown in Fig. 14. Recently, the electronic structures of $InMO_4$ (M = V, Nb, and Ta) and $BiVO_4$ were reported by Oshikiri et al. [50] according to the first principles calculations. The conduction band of $InMO_4$ (M = V, Nb, and Ta) was mainly composed of a dominant *d*-orbital component of V 3*d*, Nb 4*d*, or Ta 5*d* orbital, respectively. The valence band of $BiVO_4$ was composed of a small Bi 6*s* orbital component and a dominant O 2*p* orbital component. The band structures of Y_2GaSbO_7 and Y_2YbSbO_7 should be similar to those of $InMO_4$ (M = V, Nb, and Ta) and $BiVO_4$. Therefore, we concluded that the conduction band of Y_2GaSbO_7 was composed of Y 4*d*, Ga 4*p* and Sb 5*p* orbitals, and the valence band of Y_2GaSbO_7 was composed of a small dominant O 2*p* orbital component. Similarly, the conduction band of Y_2YbSbO_7 was composed of Y 4*d*, Yb 4*f*, and Sb 5*p* orbitals, and the valence band of Y_2YbSbO_7 was composed of a small dominant O 2*p* orbital component. Direct absorption of photons by Y_2GaSbO_7 or Y_2YbSbO_7 could produce electron–hole pairs in the photocatalyst, indicating that the larger energy than the band gap was necessary for decomposing RhB, MB, or NR by photocatalysis.

Conclusions

Y_2GaSbO_7 and Y_2YbSbO_7 were prepared by solid state reaction method for the first time. The structural, optical absorption and photocatalytic properties of Y_2GaSbO_7 and Y_2YbSbO_7 were investigated and compared with those of Bi_2InTaO_7. XRD results indicated that Y_2GaSbO_7 crystallized with the pyrochlore-type structure, cubic crystal system and space group *Fd3m*. XRD results indicated that the orthorhombic fluorite-related compound Y_2YbSbO_7 with a space group $C222_1$ was obtained. The lattice parameter *a* for Y_2GaSbO_7 was found to be 10.17981(1) Å, and the lattice parameters for Y_2YbSbO_7 were found to be $a = 10.49741(9)$ Å, $b = 7.45088(3)$ Å, $c = 7.47148(7)$ Å, respectively. The band gaps of Y_2GaSbO_7 and Y_2YbSbO_7 were estimated to be about 2.245 and 2.521 eV. Fast photocatalytic decomposition rate of aqueous RhB solutions was observed under visible light irradiation in the presence of Y_2GaSbO_7 or Y_2YbSbO_7 accompanied with the formation of end products such as carbon dioxide and water. Entire mineralization of RhB was obtained as indicated from TOC measurements. Thus the Y_2GaSbO_7/Y_2YbSbO_7-visible light system might be regarded as an effective way to remove organic dyes from the textile industry wastewater. Y_2GaSbO_7 or Y_2YbSbO_7 also showed higher photocatalytic activity than Bi_2InTaO_7 for RhB degradation. The

photocatalytic degradation of RhB followed the first-order reaction kinetics and the first-order rate constant, k, was 0.01817, 0.01341, or 0.00329 min^{-1} with Y_2GaSbO_7, Y_2YbSbO_7 or Bi_2InTaO_7 as photocatalyst. The possible photocatalytic degradation pathway of RhB was revealed under visible light irradiation. MB and NR could be degraded efficiently with Y_2GaSbO_7 or Y_2YbSbO_7 as photocatalyst under visible light irradiation.

Acknowledgments This work was supported by the National Natural Science Foundation of China (No.20877040). This work was supported by a grant from the Technological Supporting Foundation of Jiangsu Province (No. BE2009144). This work was supported by a grant from China-Israel Joint Research Program in Water Technology and Renewable Energy (No. 5).

References

1. Horikoshi S, Hojo F, Hikaka H, Serpone N (2004) Environ Sci Technol 38:2198
2. Fu HB, Pan CS, Yao WQ, Zhu YF (2005) J Phys Chem B 109:22432
3. Rehman S, Ullah R, Butt AM, Gohar ND (2009) J Hazard Mater 170:560
4. Yoon KH, Noh JS, Kwon CH, Muhammed M (2006) Mater Chem Phys 95:79
5. Pipelzadeh E, Babaluo AA, Haghighi M, Tavakoli A, Derakhshan MV, Behnami AK (2009) Chem Eng J 155:660
6. Vijayabalan A, Selvam K, Velmurugan R, Swaminathan M (2009) J Hazard Mater 172:914
7. Prairie MR, Evans LR, Stange BM, Martinez SL (1993) Environ Sci Technol 27:1776
8. Ravichandran L, Selvam K, Krishnakumar B, Swaminathan M (2009) J Hazard Mater 167:763
9. Pekakis PA, Xekoukoulotakis NP, Mantzavinos D (2006) Water Res 40:1276
10. Kansal SK, Singh M, Sud D (2007) J Hazard Mater 141:581
11. Aronson BJ, Blanford CF, Stein A (1997) Chem Mater 9:2842
12. Ghosh JP, Sui RH, Langford CH, Achari G, Berlinguette CP (2009) Water Res 43:4499
13. Kong JZ, Li AD, Zhai HF, Li H, Yan QY, Ma J, Wu D (2009) J Hazard Mater 171:918
14. Marto J, Marcos PS, Trindade T, Labrincha JA (2009) J Hazard Mater 163:36
15. Asahi R, Morikawa T, Ohwaki T, Taga Y (2001) Science 293:269
16. Sohn YS, Smith YR, Misra M, Subramanian V (2008) Appl Catal B 84:372
17. Ullah R, Dutta J (2008) J Hazard Mater 156:194
18. Jiang YH, Sun YM, Liu H (2008) Dyes Pigments 78:77
19. Luan JF, Cai HL, Zheng SR, Hao XP, Luan GY, Wu XS, Zou ZG (2007) Mater Chem Phys 104:119
20. Mohamed MM, Al-Esaimi MM (2006) J Mol Catal A 255:53
21. Li YY, Yao SS, Xue LH, Yan YW (2009) J Mater Sci 44:4455. doi:10.1007/s10853-009-3673-7
22. Dong SH, Xu KJ, Tian GS (2009) J Mater Sci 44:2548. doi:10.1007/s10853-009-3332-z
23. Wang SB, Li HT (2005) J Hazard Mater 126:71
24. Vinodgopal K, Wynkoop DE, Kamat PV (1996) Environ Sci Technol 30:1660
25. Im JS, Kim MI, Lee YS (2008) Mater Lett 62:3652
26. Horikoshi S, Hidaka H, Serpone N (2002) Environ Sci Technol 36:1357
27. Wu JM, Zhang TW (2004) J Photochem Photobiol A 162:171
28. Asilturk M, Sayilkan F, Erdemoglu S, Akarsu M, Sayilkan H, Erdemoglu M, Arpac E (2006) J Hazard Mater 129:164
29. Wu JM (2007) Environ Sci Technol 41:1723
30. Li X, Ye JH (2007) J Phys Chem C 111:13109
31. Cho IS, Lee S, Noh JH, Choi GK, Jung HS, Kim DW, Hong KS (2008) J Phys Chem C 112:18393
32. Wu TX, Liu GM, Zhao JC, Hidaka H, Serpone N (1998) J Phys Chem B 102:5845
33. Li JP, Zhang X, Ai ZH, Jia FL, Zhang LZ, Lin J (2007) J Phys Chem C 111:6832
34. Luan JF, Zhao W, Feng JW, Cai HL, Zheng Z, Pan BC, Wu XS, Zou ZG, Li YM (2009) J Hazard Mater 164:781
35. Luan JF, Hao XP, Zheng SR, Luan GY, Wu XS (2006) J Mater Sci 41:8001. doi:10.1007/s10853-006-0869-y
36. Moon J, Takagi H, Fujishiro Y, Awano M (2001) J Mater Sci 36:949. doi:10.1023/A:1004819706292
37. Zhou JK, Zhang YX, Zhao XS, Ray AK (2006) Ind Eng Chem Res 45:3503
38. Pal M, Pal U, Gonzalez RS, Mora ES, Santiago P (2009) J Nano Res 5:193
39. Marugán J, Hufschmidt D, Sagawe G, Selzer V, Bahnemann D (2006) Water Res 40:833
40. Sakthivel S, Shankar MV, Palanichamy M, Arabindoo B, Bahnemann DW, Murugesan V (2004) Water Res 38:3001
41. Izumi F (1985) J Crystallogr Assoc Jpn 27:23
42. Hinatsu Y, Ebisawa H, Doi Y (2009) J Solid State Chem 182:1694
43. Zou ZG, Ye JH, Arakawa H (2000) J Mater Sci Lett 19:1909
44. Tauc J, Grigorovici R, Vancu A (1966) Phys Status Solidi 15:627
45. Butler MA (1977) J Appl Phys 48:1914
46. Liu G, Wu T, Zhao J, Hidaka H, Serpone N (1999) Environ Sci Technol 33:2081
47. Horikoshi S, Saitou A, Hidaka H, Serpone N (2003) Environ Sci Technol 37:5813
48. Nasr C, Vinodgopal K, Fisher L, Hotchandani S, Chattopadhyay AK, Kamat PV (1996) J Phys Chem 100:8436
49. Wiegel M, Middel W, Blasse G (1995) J Mater Chem 5:981
50. Oshikiri M, Boero M, Ye JH, Zou ZG, Kido G (2002) J Chem Phys 117:7313